

See discussions, stats, and author profiles for this publication at: <https://www.researchgate.net/publication/226362547>

An electro-diffusion model for computing membrane potentials and ionic concentrations in branching dendrites, spines and axons

Article in *Biological Cybernetics* · November 1989

DOI: 10.1007/BF00217656

CITATIONS

68

READS

29

2 authors, including:



Terrence Sejnowski

Salk Institute

884 PUBLICATIONS 71,066 CITATIONS

SEE PROFILE

An Electro-Diffusion Model for Computing Membrane Potentials and Ionic Concentrations in Branching Dendrites, Spines and Axons

Ning Qian and T. J. Sejnowski

Computational Neurobiology Laboratory, The Salk Institute, P.O. Box 85800, San Diego, CA 92138-9216, USA

Abstract. The Nernst-Planck equation for electro-diffusion was applied to axons, dendrites and spines. For thick processes ($1\ \mu\text{m}$) the results of computer simulation agreed accurately with the cable model for passive conduction and for propagating action potentials. For thin processes ($0.1\ \mu\text{m}$) and spines, however, the cable model may fail during transient events such as synaptic potentials. First, ionic concentrations can rapidly change in small compartments, altering ionic equilibrium potentials and the driving forces for movement of ions across the membrane. Second, longitudinal diffusion may dominate over electrical forces when ionic concentration gradients become large. We compare predictions of the cable model and the electro-diffusion model for excitatory postsynaptic potentials on spines and show that there are significant discrepancies for large conductance changes. The electro-diffusion model also predicts that inhibition on small structures such as spines and thin processes is ineffective. We suggest a modified cable model that gives better agreement with the electro-diffusion model.

1 Introduction

The cable model of electrical conduction is central to our understanding of information processing in neurons. The conduction of action potentials in axons has been modeled as a nonlinear excitable cable (Hodgkin and Huxley 1952) and the integration of postsynaptic signals in dendrites has been studied with analytic solutions to passive cables (Rall 1977). Recently, several groups have used the cable model to examine the possibility of more complex signal processing in dendrites with complex morphologies, multiple synaptic inputs, and passive or excitable mem-

branes (Shepherd et al. 1985; Koch and Poggio 1983; Koch et al. 1983; Rall and Segev 1987; Perkel and Perkel 1985; Wathey et al. 1989).

The resting membrane potential is maintained by ionic concentration differences across the membrane. In the cable model, the equilibrium potential of each ion is represented by a battery whose electromotive force is given by the Nernst potential. Changes in the membrane permeability are modeled by changes to conductances in series with the batteries. The ionic concentrations are usually not significantly altered by these conductance changes, so the equilibrium potentials are not altered and the potentials of the batteries can be considered fixed. However, there are circumstances when this is not a good assumption. If the intracellular volume is relatively small, as in dendritic spines, then ionic concentrations can change rapidly following a transient change in ionic conductances. Moreover, a sudden change in concentration at one location can lead to gradients of ionic concentration within a thin process, which violates another fundamental assumption of the cable model. Under these circumstances, it is necessary to consider the fundamental laws governing the movements of ions, as given by the Nernst-Planck equations for electro-diffusion (Jack et al. 1975).

There is another motivation for carefully treating the ionic concentrations and the diffusion of ions within neurons. Many intracellular functions are regulated by concentrations of particular ions. For example, the release of neurotransmitter depends on the concentration of Ca^{2+} inside presynaptic terminals, which can change by an order of magnitude in milliseconds (Stockbridge and Moore 1984; Fogelson and Zucker 1985; Simon and Llinas 1985). The inflow of Ca^{2+} into postsynaptic dendrites precedes the induction long-term potentiation in hippocampal pyramidal cells (Malenka et al. 1988). Thus, it is important to predict accurately the concentration changes of

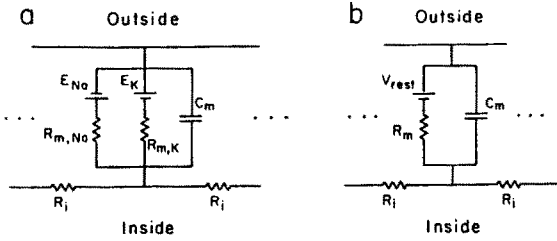


Fig. 1. **a** Electrical circuit for one compartment in cable model for a neuronal process and **b** an equivalent circuit. Only K^+ and Na^+ are considered in this model

Ca^{2+} in small compartments such as synaptic boutons and dendritic spines.

In this paper we introduce an electro-diffusion model for small compartments and thin processes that is based on the Nernst-Planck equation. The electro-diffusion model provides a unified framework for the computation of both the membrane potentials and the intracellular ionic concentrations during synaptic activation. Some preliminary results for excitatory postsynaptic potentials have already been reported (Qian and Sejnowski 1988). We extend the model to inhibitory postsynaptic potentials and show that inhibition is not effective on spines and thin dendrites (Qian and Sejnowski 1989).

2 Limitations of the Cable Model

In the cable model, the membrane potential, $V(z, t)$, at distance z and time t along a cable obeys the equation (Jack et al. 1975):

$$\frac{d}{4R_i} \frac{\partial^2 V}{\partial z^2} = C_m \frac{\partial V}{\partial t} + I_m, \quad (1)$$

where d is the diameter of the cable, R_i ($\Omega \text{ cm}$) is the total intracellular cytoplasmic resistivity, C_m ($\mu\text{F}/\text{cm}^2$) is the membrane capacitance per unit area, and I_m (mA/cm^2) represents the total non-capacitative membrane current density which is the summation of all non-capacitative membrane current densities for each ionic species, $I_{m,k}$. If we assume that the movement of ionic species k across the membrane can be described by a membrane resistance of unit area $R_{m,k}$ ($\Omega \text{ cm}^2$) in series with a battery whose electromotive force E_k is equal to the ionic equilibrium potential as shown schematically in Fig. 1a, then

$$I_{m,k} = (V - E_k) / R_{m,k}, \quad (2)$$

and

$$I_m = \sum_k I_{m,k} = (V - V_{\text{rest}}) / R_m. \quad (3)$$

where the resting membrane potential, V_{rest} , and the total membrane resistance, R_m , are given by:

$$V_{\text{rest}} = R_m \sum_k (E_k / R_{m,k})$$

$$1/R_m = \sum_k (1/R_{m,k}).$$

Through these definitions, the electrical circuit in Fig. 1a can be reduced to the equivalent circuit shown in Fig. 1b. The standard equation for the cable model is obtained by substituting (3) into (1), assuming that V is measured from the resting potential V_{rest} (Rall 1977):

$$\lambda^2 \frac{\partial^2 V}{\partial z^2} = \tau_m \frac{\partial V}{\partial t} + V, \quad (4)$$

where the space and time constants are defined as

$$\lambda = (dR_m/4R_i)^{1/2},$$

$$\tau_m = R_m C_m.$$

The electromotive forces of the membrane batteries (equilibrium potentials) in the cable model are usually obtained from the Nernst equation and are considered constants. This is a good approximation in the squid giant axon or other large neurons, but may introduce errors if the concentrations of some ions change significantly with time. This applies to Ca^{2+} concentrations in many situations and to synaptic events in small structures such as dendritic spines (Rall 1978; Koch and Poggio 1983). Restricted extracellular spaces may also result in significant extracellular ionic concentration changes (see Discussion).

A second limitation of the cable model is in the treatment of longitudinal spread of current within neurons. In the cable model, the gradient of the electrical potential in the cytoplasm is the driving force for the ionic current, but there is no provision for the driving forces due to concentration gradients. This is usually a good assumption, but it may not be valid for ions like Ca^{2+} and for small structures like dendritic spines where the spatial concentration gradients can be very large.

Finally, different ions may have different concentration-dependent cytoplasmic resistivities [see (13)], but the cable model only incorporates the total cytoplasmic resistivity. This may not be a valid approximation when the concentrations of ions are changing differentially. In summary, one expects that the cable model may not be appropriate when spatial and/or temporal ionic concentrations changes are large and especially when ionic concentration changes need to be determined.

In the following sections we will first derive a set of equations that govern the electrodiffusion of ions in neuronal processes and discuss their relationship with the cable model. We will then present numerical

solutions to these equations for a propagating action potential in a long axon and for postsynaptic potentials in a dendritic spine. A modified cable model is proposed which agrees well with the electrodiffusion model when the ionic concentration are not changing too quickly. Finally, we discuss the origin of the differences between the electro-diffusion model and the cable model and the effects of restricted extracellular space, ionic pumps and ionic exchangers in the membrane.

3 Electro-Diffusion Model

The movement of ions in neurons is governed by the Nernst-Planck equation (Jack et al. 1975):

$$\bar{J}_k = -D_k(\bar{\nabla}n_k + (n_k/\alpha_k)\bar{\nabla}V), \quad (5)$$

where V is the potential, \bar{J}_k is the flux of ionic species k (number of particles per unit area), D_k is the diffusion constant, n_k is the concentration, and the constant α_k is defined as

$$\alpha_k = RT/Fz_k,$$

where z_k is the valence of ionic species k , R is the gas constant, F is the Faraday constant, and T is the absolute temperature. The ionic concentrations and ionic currents must additionally satisfy the continuity equation:

$$\bar{\nabla} \cdot \bar{J}_k + \frac{\partial n_k}{\partial t} = 0. \quad (6)$$

Consider a cylinder of diameter d and assume that the longitudinal current and ionic concentrations are uniform across the transverse cross-section of the cylinder. Assume also that transverse currents occur only at the surface of the cylinder and are independent of angle around the axis of the cylinder. These assumptions reduce the problem of electro-diffusion to a one-dimensional problem along the axis of the cylinder. The equations can be written in cylindrical coordinates and reduced to a single equation for the concentration as a function of the distance along the z -axis of a cylinder:

$$\frac{\partial n_k}{\partial t} = D_k \frac{\partial^2 n_k}{\partial z^2} + \frac{D_k}{\alpha_k} \frac{\partial}{\partial z} \left(n_k \frac{\partial V}{\partial z} \right) - \frac{4}{d} J_{m,k}, \quad (7)$$

where $J_{m,k}$ is the membrane flux of ionic species k , positive for outgoing flux (see the Appendix for details of the derivation). An expression for the membrane fluxes can be obtained by making the constant-field approximation for the q component of (5) (Goldman 1943):

$$J_{m,k} = \frac{P_k V}{\alpha_k} \left[\frac{n_k^{\text{out}} - n_k \exp(V/\alpha_k)}{1 - \exp(V/\alpha_k)} \right]. \quad (8)$$

The Eq. (7) becomes:

$$\frac{\partial n_k}{\partial t} = D_k \frac{\partial^2 n_k}{\partial z^2} + \frac{D_k}{\alpha_k} \frac{\partial}{\partial z} \left(n_k \frac{\partial V}{\partial z} \right) - \frac{4P_k V}{\alpha_k d} \left[\frac{n_k^{\text{out}} - n_k \exp(V/\alpha_k)}{1 - \exp(V/\alpha_k)} \right], \quad (9)$$

where P_k is the permeability of the membrane and n_k^{out} is the concentration of ionic species k outside the membrane, which was considered constant for all simulations reported in this paper. The three terms on the right-hand side of this equation are, respectively, the contributions from pure diffusion, the potential gradient, and the membrane current. In applying (9) to some problems, the last term may be replaced by an experimentally-determined expression for the membrane current to eliminate the error introduced by the constant-field approximation.

Equation (2) has been found to be a good approximation for squid giant axons (Hodgkin and Huxley 1952) while (8) better describes the membrane currents in the myelinated nerve fibers of *Xenopus laevis* (Frankenhaeuser and Huxley 1964). It is not clear whether (8) or (2) is a better approximation for dendritic spines, especially when changes in ionic concentrations are large. The expressions for the membrane currents of ionic species k in (2) and (8) cannot be made equivalent even when the ionic concentrations are almost constant. An additional requirement is that the membrane potential V should be very close to the equilibrium potential of ions, which obviously cannot be satisfied for all ions at the same time. The constant-field approximation in (8) was used in our model because it at least takes concentrations explicitly into account. In a later section we show that if the ionic concentrations change and the equilibrium E_k in (2) are updated according to the Nernst equation, then the modified cable model based on (2) gives results similar to the electro-diffusion model based on (8).

Equation (9) must be supplemented by an additional constraint between the membrane potential and the ionic concentrations. We adopt the same capacitive model of the membrane used in the cable model; that is, we assume that the potential change in a short segment of a process is equal to the change of the total charge in the segment divided by its membrane capacitance:

$$V(z, t) = V_{\text{rest}} + (Fd/4C_m) \sum_k [n_k(z, t) - n_{k,\text{rest}}] z_k, \quad (10)$$

where V_{rest} is the initial potential and $n_{k,\text{rest}}$ is the initial ionic concentration of species k .

Neuronal processes often branch and change their diameters. If branches are allowed, then these equations must be solved on a tree rather than a line.

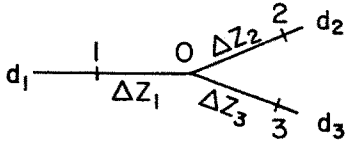


Fig. 2. A branch point of a neuronal process with diameter jumps. The three sample points are labeled 1, 2, and 3 around the branch point 0. The diameters for the three branches are d_1 , d_2 , and d_3 respectively. Δz_1 , Δz_2 , and Δz_3 represent the spatial distances between point 0 and points 1, 2, and 3 respectively

Continuous diameter changes can be approximated by segments having piecewise constant diameters. At points where the diameter jumps and/or branches occur, the solutions can be matched using the continuity of flux at that point. The continuity constraint at a branch point can be derived from (5). For the geometry illustrated in Fig. 2 where both branching and diameter jumps occur, the continuity constraint at point 0 is:

$$d_1^2 \left(\frac{\partial n_k}{\partial z} + \frac{n_k}{\alpha_k} \frac{\partial V}{\partial z} \right) \Big|_1 = d_2^2 \left(\frac{\partial n_k}{\partial z} + \frac{n_k}{\alpha_k} \frac{\partial V}{\partial z} \right) \Big|_2 + d_3^2 \left(\frac{\partial n_k}{\partial z} + \frac{n_k}{\alpha_k} \frac{\partial V}{\partial z} \right) \Big|_3. \quad (11)$$

The square of the diameter enters into this equation because the flux through the areas of each branch must be matched. There is an analytic solution of the cable model for branching dendrites having passive membranes if Rall's "3/2 power law" (Rall 1977) is satisfied. This law for an equivalent cylinder does not hold for our electro-diffusion model except in the limit when the concentration gradients go to zero and (2) rather than (8) is used to compute the membrane currents. A compartment approximation for the solution of (9) is inaccurate for large ionic fluxes if the continuity

constraint in (11) is not used to match solutions on the two sides of a diameter jump or at a branch point.

Note that (9) requires that both the potentials and the ionic concentrations be continuous with respect to z (otherwise the derivatives would become infinite). However, by (10) the potential is not continuous at a diameter jump if the ionic concentrations are continuous. This is the artifact of assuming a sudden diameter change and can be resolved by setting the voltage at the jump to the average of the voltages on either side (see Appendix).

The differential equations in (9) coupled through (10) were converted to finite difference equations and were integrated by a first-order forward Euler approximation (Mascagni 1989). The solutions at diameter jumps and/or branching points were obtained by solving the coupled nonlinear algebraic equations derived from the matching conditions in (11). The details of these numerical methods are described in the Appendix.

4 Relationship Between the Electro-Diffusion Model and the Cable Model

In large neuronal processes the internal and external ionic concentrations are likely to remain approximately constant during a transient membrane conductance change. If the concentration gradients are small, the contribution due to the diffusion of ions within the neuron becomes negligible and the longitudinal current is purely resistive. It can be shown (see Appendix) that (7) and (10) then reduce to the form in (1). Thus, the electro-diffusion model in the limiting case is identical to cable model in calculating the membrane potential V if the same membrane currents are used.

Table 1. Parameters used in the electro-diffusion model. The diffusion constants were taken from Hille (1984). The membrane capacitance follows Koch and Poggio (1983) to facilitate comparisons. The determination of the other parameters is discussed in the text

Symbol	Value	Parameter
D_K	$1.96 \times 10^{-5} \text{ cm}^2/\text{s}$	Diffusion coefficient for K^+
D_{Na}	$1.33 \times 10^{-5} \text{ cm}^2/\text{s}$	Diffusion coefficient for Na^+
$P_{K,rest}$	$3.64 \times 10^{-6} \text{ cm/s}$	Resting permeability of K^+
$P_{Na,rest}$	$6.07 \times 10^{-8} \text{ cm/s}$	Resting permeability of Na^+
$[K]_{in}(0)$	140 mM	Initial internal K^+ concentration
$[Na]_{in}(0)$	12 mM	Initial Na^+ concentration
$[K]_{out}$	4 mM	External K^+ concentration
$[Na]_{out}$	145 mM	External Na^+ concentration
$P_{Na,M}$	$6.07 \times 10^{-3} \text{ cm/s}$	Maximum Na^+ permeability of spine
t_p	1 ms	Time to reach peak permeability
T	20°C	Temperature
C_m	$2 \mu\text{F}/\text{cm}^2$	Membrane capacitance per unit area

Table 2. Parameters used in the cable model. R_i was calculated from (8) and (9), E_K and E_{Na} were calculated from the intracellular and extracellular $[K^+]$ and $[Na^+]$ respectively according to Nernst equation, and $R_{m,K}$ and $R_{m,Na}$ were determined from P_K and P_{Na} by setting the resting K^+ and Na^+ currents equal to those in the electro-diffusion model. This automatically made the resting potentials the same in two models. There were no free parameters left in the cable model

Symbol	Value	Parameter
R_i	89.9 Ω cm	Total cytoplasmic resistivity
$R_{m,K}$	$4.33 \times 10^3 \Omega$ cm ²	Resting membrane resistance of K^+ of unit area
$R_{m,Na}$	$5.15 \times 10^4 \Omega$ cm ²	Resting membrane resistance of Na^+ of unit area
E_K	-89.8 mV	K^+ equilibrium potential
E_{Na}	62.9 mV	Na^+ equilibrium potential
$G_{Na,M}$	1.94 S/cm ²	Maximum Na^+ conductance of spine head per unit area
t_p	1 ms	Time to reach peak conductance
C_m	2 μ F/cm ²	Membrane capacitance per unit area

A relationship can be derived between parameters in two models (see Appendix):

$$1/R_i = \sum_k (1/R_{i,k}), \quad (12)$$

$$1/R_{i,k} = (F^2/RT) D_k n_k z_k^2, \quad (13)$$

where R_i is the total resistivity of the cytoplasm and $R_{i,k}$ are the ionic resistivities for each species of ion. For the squid cytoplasm, $[K^+] = 400$ mM, $[Na^+] = 50$ mM, and for the T and D_k given in Table 1, the estimated resistivities are $R_{i,K} = 33.4 \Omega$ cm and $R_{i,Na} = 267 \Omega$ cm. There is a significant difference between the resistivities of the individual ionic species. The total cytoplasmic resistivity is $R_i = 29.7 \Omega$ cm. The change of R_i with concentration during a synaptic potential in a dendritic spine can be large and are shown in Fig. 8. When Ca^{2+} concentrations change by several orders of magnitude following the influx of Ca^{2+} into a cell, $R_{i,Ca}$ can change dramatically because it is inversely related to the Ca^{2+} concentration by (13).

5 Modeling Action Potentials

The cable model has been successful in modeling action potentials when the appropriate expressions for the membrane currents are used. We tested our numerical solution of the electro-diffusion model by generating an action potential for the squid giant axon using the active membrane currents given by Hodgkin and Huxley (1952) [These are based on (2) and accurately describe the experimental data. We did not use a constant field approximation because the corresponding parameters for the experimental data were not available]. The results, shown in Fig. 3, are indistinguishable from those of the electrical conductance model (Cooley and Dodge 1966) because the ionic concentrations changes are extremely small during the process. When an axon with a diameter of 1μ m was

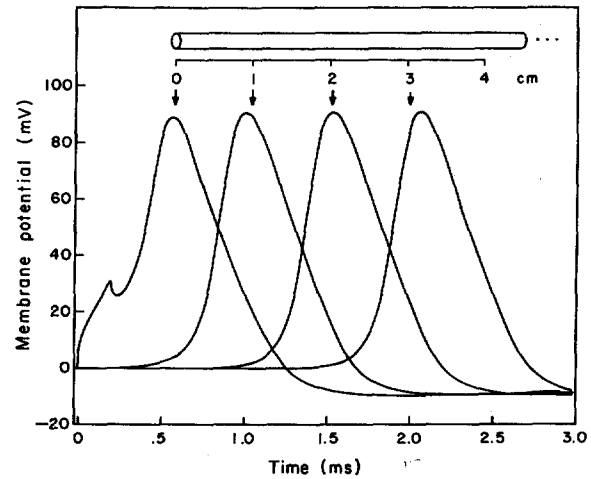


Fig. 3. Electro-diffusion model of a propagating action potentials in the squid giant axon. Membrane currents were based on those given by Hodgkin and Huxley (1952). The results are indistinguishable from the predictions of the cable model (Cooley and Dodge 1966). $D_K = 5.11 \times 10^{-5}$ cm²/s and $D_{Na} = 3.47 \times 10^{-5}$ cm²/s so that (12) is satisfied. All of the other parameters are the same as those used by Cooley and Dodge (1966)

used, the maximum relative concentration change was only about 1.4%. We expect that even a high-frequency train of action potentials (300 Hz) will not cause significant concentration changes if ionic pumps and exchange mechanisms are working (see Discussion). However, for axons as small as 0.1μ m, the electro-diffusion model departs significantly from the cable model.

6 Modeling an Excitatory Postsynaptic Potential in a Dendritic Spine

Many vertebrate and invertebrate neurons receive synaptic inputs on spines (Coss and Perkel 1985).

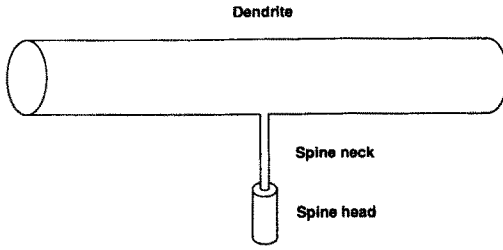


Fig. 4. Geometry of a model dendritic spine. The spine was located in the center of a dendrite with total length 300 μm and diameter 1 μm ; the spine neck was 1 μm long and 0.1 μm in diameter; the spine head was 0.69 μm long and 0.3 μm in diameter

Because of the small size of dendritic spines, postsynaptic potentials can be accompanied by significant changes in the internal ionic concentrations. In this section we simulate an excitatory postsynaptic potential on a spine using the electro-diffusion model and compare the results with the conventional cable model. For simplicity, only two types of ions, K^+ and Na^+ , will be considered in this paper.

The morphology of the dendritic spine used in the simulations is shown in Fig. 4 (adapted from Koch and Poggio 1983). The total surface area of the spine head was 0.65 μm^2 , neglecting the area at the ends of the cylinders. The synaptic input was modeled by adding a transient change in the resting Na^+ permeability of the membrane (Koch and Poggio 1983):

$$P_{\text{Na}}(t) = P_{\text{Na},M} (et/t_p)^\alpha e^{-at/t_p}, \quad (14)$$

where $P_{\text{Na},M}$ is the maximum change in Na^+ permeability, t_p is the time to reach peak, and e is the base of the natural logarithms. We follow the convention in Koch and Poggio (1983) and choose $\alpha=4$, which is smooth at $t=0$. For $\alpha=1$ this function has a positive slope at $t=0$ and is called the α -function by Rall (1967).

Table 1 summarizes the parameters used in our simulations of spines using the electro-diffusion model. We chose the membrane parameters so that the resting membrane potentials and resting membrane currents were the same as those in the cable model. The ionic membrane resistances for K^+ and Na^+ in cable model were determined from the total membrane resistance of about 4000 Ωcm^2 and the resting membrane potential of about -78 mV . Permeabilities were determined from membrane resistances by equating the resting currents of K^+ and Na^+ in two models.

The membrane potential change from the resting level during a simulated excitatory postsynaptic potential is shown in Fig. 5. At the peak of the response the Na^+ permeability increased by 10^5 over the resting membrane Na^+ permeability. The concomitant changes in the ionic concentration of K^+ are shown in Fig. 6. The changes of the Na^+ concentration (not

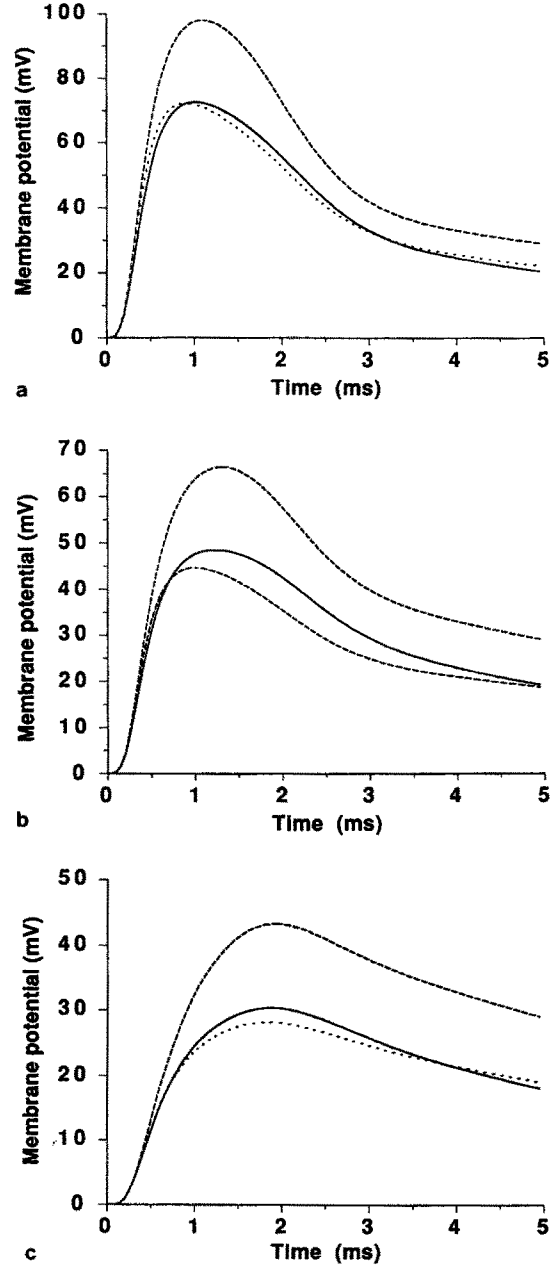


Fig. 5a–c. Excitatory postsynaptic potential from the resting level (-78 mV) as a function of time at **a** the middle of the spine head, **b** the middle of the spine neck, and **c** the dendritic shaft at the base of the spine, modeled by the electro-diffusion model (solid line), the standard cable model (dashed line) and the modified cable model (dotted line). The parameters in these models are given in Tables 1 and 2

shown) were almost mirror images of those for K^+ ; that is, they had about the same amplitude but opposite sign. A small change in the total concentration of K^+ and Na^+ causes a very large potential change because the membrane capacitance is quite small.

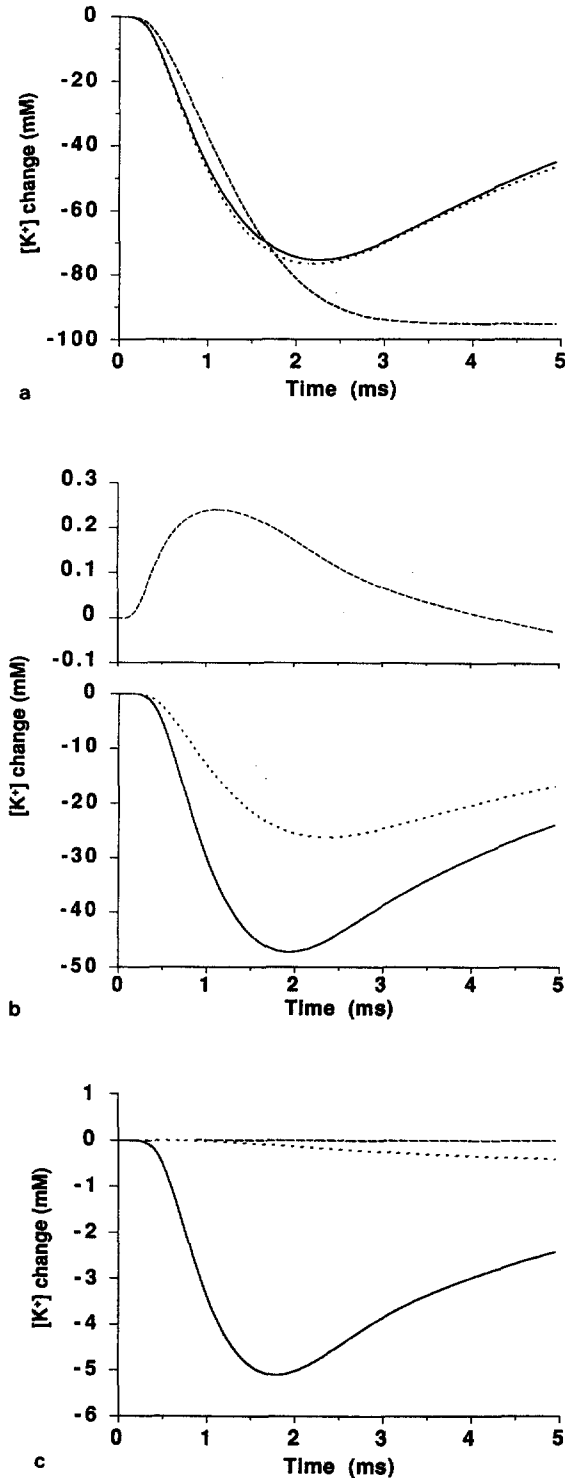


Fig. 6a–c. Changes of the intracellular K^+ concentration from the resting level (140 mM) during an excitatory postsynaptic potential at **a** the middle of the spine head, **b** the middle of spine neck, and **c** the dendritic shaft at the base of the spine as predicted by three models: The electro-diffusion model (solid line), the standard cable model (dashed line) and the modified cable model (dotted line). The parameters in these models are given in Tables 1 and 2

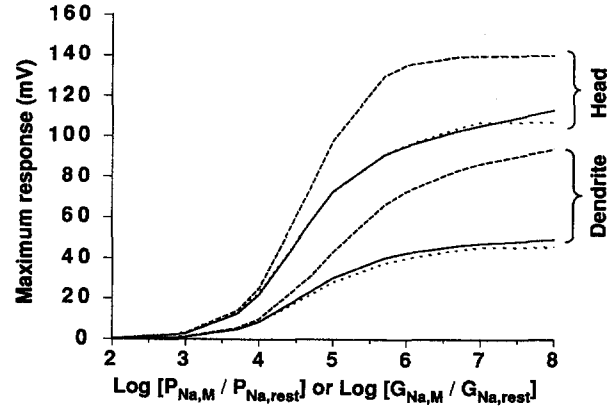


Fig. 7. Maximum response of an excitatory postsynaptic potential from the resting level (-78 mV) at the spine head and the dendritic shaft at the base of the spine as predicted by three models: The cable model (dashed line) and the modified cable model (dotted line) as functions of the maximum conductance change relative to the resting Na^+ conductance, and the electro-diffusion model (solid line) as a function of the maximum permeability change relative to the resting Na^+ permeability. $G_{Na,rest}$ is the resting membrane conductance per unit area and is equal to the inverse of $R_{m,Na}$ in Table 2

There are indeed significant concentration changes in the spine compared to the resting concentration values and it is therefore incorrect to assume that the Nernst potentials remain constant, as in the cable model. In Fig. 7, the maximum excitatory postsynaptic potentials in the spine head and in the dendritic shaft at the base of spine are shown as functions of the maximum sodium permeability over its resting value. The present model does not take into account the effects of limited extracellular space, such as extracellular K^+ accumulation. The consequences of including these effects is pointed out in the Discussion.

The results of the electro-diffusion model were compared with an equivalent cable model of the spine. The parameters given in Table 2 for the cable model were chosen to match those in Table 1 for the electro-diffusion model. The transient change in the membrane conductance per unit area of Na^+ from its resting values at the spine head during the synaptic input was modeled by

$$G_{Na}(t) = G_{Na,M} (et/t_p)^\alpha e^{-\alpha t/t_p}, \quad (15)$$

where we chose $\alpha = 4$ to match the functional form of the permeability changes in (14). $G_{Na,M}$ is the maximum Na^+ conductance per unit area and was chosen by setting its ratio to the resting Na^+ conductance per unit area $G_{Na,rest}(1/R_{m,Na})$ equal to $P_{Na,M}/P_{Na,rest}$ in the electro-diffusion model. The t_p and C_m were same as those in the electro-diffusion model.

The ionic concentrations are normally assumed to remain constant in the cable model. However, it is

possible to compute the concentrations that are implicit in the cable model by integrating the currents flowing into each compartment for each ionic species:

$$\Delta n_k = \int_0^t I_k dt, \quad (16)$$

where I_k is the total current of species k entering a compartment. Figures 5 and 6 show the time course of the membrane potential and K^+ concentration changes predicted by the cable model together with the results of electro-diffusion model. The maximum response of the membrane potential as a function of the maximum Na^+ conductance is plotted in Fig. 7 in comparison with electro-diffusion model. For small conductance changes the two models predicted similar potential responses. However, for large conductance changes there were significant differences between the responses predicted by the cable model and the electro-diffusion model, especially at the base of the dendritic spine.

The responses predicted by the cable model saturated as the membrane potential approached the Na^+ equilibrium potential. This saturation occurred at a lower membrane potential in the electro-diffusion model because of the increase in the internal Na^+ concentration and concomitant decrease of the Na^+ equilibrium potential. The longer the duration of the excitatory synaptic potential, the larger the change in the Na^+ equilibrium potential.

The discrepancies between the ionic concentration changes predicted by the two models are larger than what one might have expected from the differences between the membrane potentials. This is best seen by comparing the calculated K^+ concentration changes in the spine neck based on the two models (Fig. 6b). There is a dramatic decrease of K^+ concentration in the spine neck according to the electro-diffusion model, while the cable model predicts that there should be a small increase. This difference can be attributed to the neglect of ionic diffusion in the cable model.

The membrane potential in the spine head is always higher than that of spine neck, so the potential gradient tends to drive ions from the head to the neck. However, the K^+ concentration in the spine head is much lower than that of spine neck due to the outflow of K^+ ions to the extracellular space; therefore, the concentration gradient tends to drive K^+ ions from the neck to the head. The concentration gradient is so large that it dominates the process and results in a net K^+ flow from neck to head.

The other major factor that influences the concentration changes in the cable model is cytoplasmic resistivity R_i . Figure 8 shows how $R_{i,K}$ and $R_{i,Na}$ change in the spine head according to (13) based on the

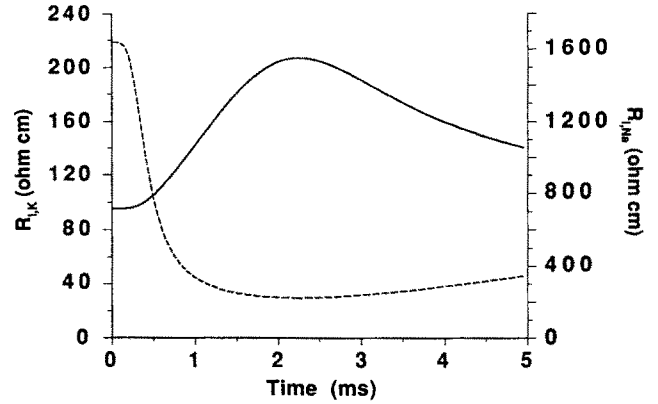


Fig. 8. Cytoplasmic resistivities for K^+ (solid line) and Na^+ (dashed line) in the spine head during the synaptic response shown in Figs. 5a and 6a

concentration changes at the spine head in Fig. 6a. These R_i 's are constant in the cable model.

Varying the Time-To-Peak

The results in Figs. 5–8 were calculated with a time-to-peak, t_p , of 1 ms. We also studied the discrepancies between the two models as a function of t_p , with all the other variables fixed to the values given in Tables 1 and 2. The maximum responses of the membrane potentials from their resting levels are shown in Fig. 9 for the spine head and the dendritic shaft at the base of the spine. As t_p was increased, the concentration changes in the spine were larger and lasted longer, which lead to larger differences between the two models. The maximum concentration changes for the electro-diffusion model are plotted as a function of t_p in the spine head in Fig. 10 in comparison with the maximum changes predicted by the cable model. (The concentration

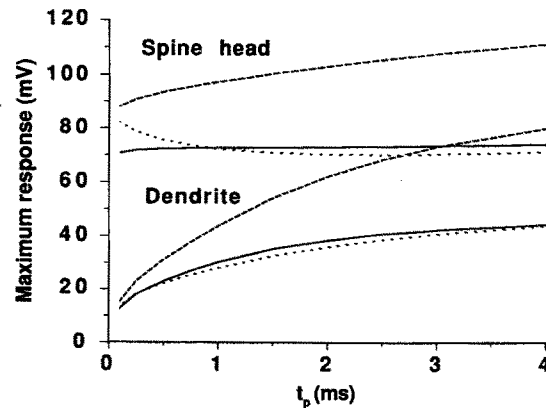


Fig. 9. Maximum excitatory postsynaptic potentials predicted by the cable model (dashed line), the modified cable model (dotted line), and the electro-diffusion model (solid line) at the spine head and the dendritic shaft at the base of the spine as functions of t_p , the time-to-peak, defined in (14) and (15)

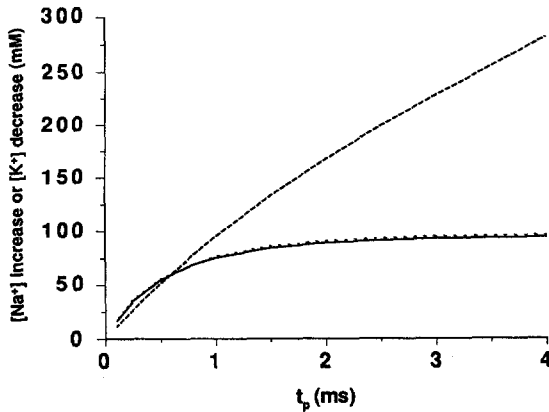
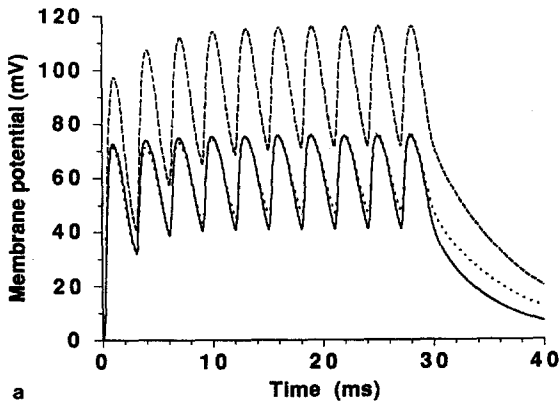
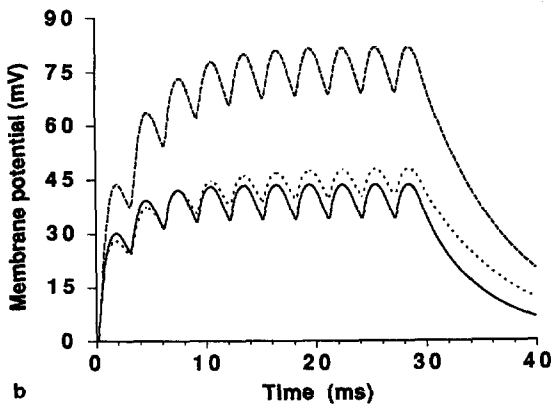


Fig. 10. Maximum changes in Na^+ and K^+ concentrations during an excitatory postsynaptic potential in the spine head from their resting levels predicted by the standard cable model (dashed line), the modified cable model (dotted line), and the electro-diffusion model (solid line) as functions of the time-to-peak, t_p .



a



b

Fig. 11. Responses to a tetanus of 10 synaptic inputs in 30 ms from a resting level of -78 mV at **a**, the middle of spine head, and **b**, the dendritic shaft at the base of the spine, predicted by the electro-diffusion model (solid line), the conventional cable model (dashed line) and the modified cable model (dotted line).

changes shown in Fig. 6a predicted by the cable model appear to be reaching a maximum asymptotically, so we used the values at $5 t_p$.) When t_p was greater than about 1.7 ms, the decrease predicted by the cable model was, unrealistically, larger than the initial K^+ concentration, which was 140 mM.

Temporal Summation

In the simulations of a dendritic spine presented above, a single synaptic activation was modeled as a transient Na^+ conductance or permeability change. A synapse on a spine may, however, receive multiple synaptic activations in close succession in response to a train of action potentials arriving at the presynaptic terminal (Gamble and Koch 1987). Temporal summation will occur when t_p is comparable to the time interval between two successive postsynaptic potentials. The ionic concentration changes in a spine during multiple synaptic activations will be larger than a single activation because of the prolonged opening of Na^+ channels, so one expects there to be a larger discrepancy between the cable model and the electro-diffusion model.

We simulated a synaptic tetanus with t_p equal to 1 ms and 10 synaptic inputs in 30 ms, with all other parameters in Tables 1 and 2 fixed. The results are shown in Fig. 11 for both the electro-diffusion model and the cable model. The discrepancy between the two models after 10 inputs is indeed much more significant than that after the first input. The magnitude of temporal summation at the dendritic shaft predicted by the cable model is much larger than that predicted by the electro-diffusion model.

7 Inhibitory Synaptic Input on Dendritic Spines

A transient conductance change with a reversal potential equal to the resting membrane potential is called silent inhibition because, according to the cable model, such a synaptic input by itself will not change the membrane potential at all; however, if the inhibition occurs during an excitatory synaptic response, the current will be shunted and the excitation will be less effective in depolarizing the membrane. If such a silent synaptic input is large and on a small structures such as a spine, the conductance may be large enough to significantly change ionic concentrations and the reversal potential of the inhibitory synapse. Thus, the silent inhibition may no longer be silent.

We applied the electro-diffusion model to this problem and modeled the silent inhibitory input with simultaneous K^+ and Na^+ permeability increases having a ratio that was the same as the resting permeabilities. The comparable combination of con-

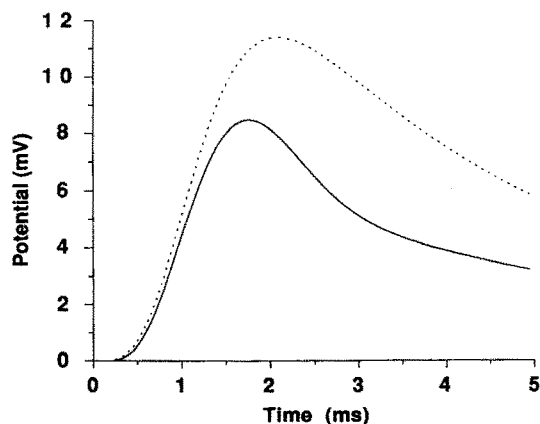


Fig. 12. Responses to silent inhibitory synaptic input at the spine head (solid line) predicted by the electro-diffusion model. The K^+ and Na^+ permeabilities changes had a ratio equal to that of their resting permeabilities so that in the standard cable model there was no response at the resting potential. The peak K^+ permeability change, $P_{K,M}$, was 6.07×10^{-2} cm/s. This apparently excitatory response is caused by a shift of the synaptic reversal potential (dotted line) from its resting level

ductance changes produces no change in potential in the cable model. Figure 12 shows that the response in the spine head predicted by the electro-diffusion simulation is excitatory, not silent as expected from the cable model. This is a consequence of the decrease in the concentration of K^+ during the response, which leads to an increase of the equilibrium potential for K^+ . If the silent inhibitory input is carried exclusively by Cl^- , a third ion whose equilibrium potential is close to the resting potential, there should be no response. As the concentration of Cl^- inside the cell rises, the driving force for the Cl^- becomes zero and there is no net current.

Interaction Between Inhibitory and Excitatory Synaptic Inputs

In their study of nonlinear interactions between excitation and inhibition using the cable model Koch and Poggio (1983) and Koch et al. (1983) conclude that a strong silent inhibitory input can effectively veto the effect of an excitatory input provided that they have the appropriate temporal and spatial relationships. We studied this type of interaction at the spine head by modeling a silent inhibitory input as described above together with an excitatory input. As shown in Fig. 13, the veto effect predicted by the electro-diffusion model is much weaker than predicted by the cable model based on comparable conductances changes.

The reduction in the effectiveness of shunting inhibition on the excitatory synapse is brought about

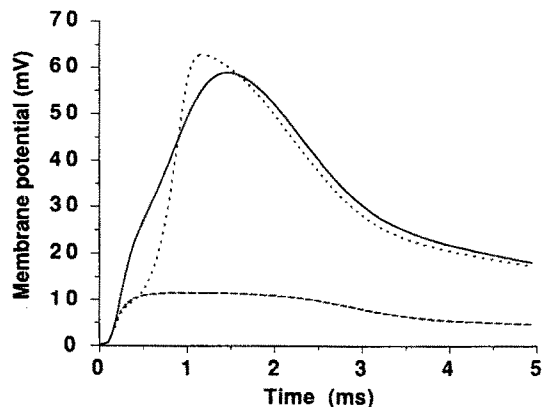


Fig. 13. Membrane potential responses to simultaneous excitatory and silent inhibitory synaptic inputs on the same spine at the middle of spine head, and the dendritic shaft at the base of the spine, predicted by three models: The electro-diffusion model (solid line), the conventional cable model (dashed line) and the modified cable model (dotted line). The amplitude of inhibition (the same as in Fig. 12) was 10 times larger than the amplitude of excitation. All other parameters are given in Tables 1 and 2. The responses at the spine head and the dendritic shaft in the absence of inhibition is given in Fig. 5a and b

mainly because the large K^+ outflow makes the Nernst potential of K^+ much more positive and therefore less inhibitory. Although we did not simulate the case when Cl^- is the source of inhibition, we would expect to obtain similar results since the depolarization and increase of Cl^- permeability would also produce a Cl^- current that would in turn make the Cl^- Nernst potential less negative. According to the electro-diffusion model, it is impossible to have a truly silent inhibition on a spine.

For an inhibitory input on a large dendrite or cell body (or for a combination of excitation and inhibition), the change in concentration at the site of inhibition is almost negligible and the veto effect predicted by the cable model remains valid. However, for thin dendrites (around $0.1 \mu m$ in diameter) the changes in concentration can be very large, and the conclusions reached for the spine are equally valid for the dendrite. We have also studied the effect of silent inhibition as a function of the relative timing between excitation and inhibition on spines and have found that the veto effect predicted from the cable model (Koch and Poggio 1983) does not occur.

8 Modifications to the Cable Model

The electro-diffusion model is highly computation intensive and cannot be used routinely for large-scale simulations of complex dendritic trees (Wathey et al. 1989). However, we found that the following modifica-

tions of the cable model allowed it to more accurately approximate the predictions of the electro-diffusion model. At each time step:

i) Calculate the intracellular concentration of each ionic species explicitly in each compartment from the membrane currents and the ionic currents flowing between compartments [see (16)].

ii) Compute the new membrane equilibrium potentials for each compartment using the intracellular and extracellular ionic concentrations according to Nernst equation and update the membrane batteries:

$$E_k = (RT/Fz_k) \ln \frac{n_k(\text{out})}{n_k(\text{in})},$$

where $n_k(\text{out})$ is the ionic concentration of species k outside the membrane and $n_k(\text{in})$ is the ionic concentration inside the membrane.

iii) Replace the single longitudinal resistance between compartments with parallel resistances $R_{i,k}$ in series with batteries for each ionic species [see (13)]. [In an earlier report (Qian and Sejnowski 1988), we did not update the cytoplasmic resistances; the update of these resistances significantly improves the modified cable model, especially for $t_p > 1$ ms.]

iv) Determine the longitudinal batteries by the Nernst potential from ionic concentrations of the two compartments they connect and update in the same way as the membrane batteries. The potential of the battery for species k between compartments j and $j+1$ is:

$$E_{i,k} = (RT/Zz_k) \ln \frac{n_k(j)}{n_k(j+1)},$$

where a positive value for $E_{i,k}$ means that the positive terminal of the battery is pointing to the $j+1$ compartment.

A schematic view of the modified cable model is represented in Fig. 14. This model was applied to the dendritic spine model in Fig. 4 and the results are shown in comparison with the electro-diffusion and cable models in Figs. 5–7, 9–11, and 13.

The agreement between the modified cable model and electro-diffusion model for predicting membrane potentials was good except for the interaction between excitatory and inhibitory inputs shown in Fig. 13. The comparisons between the predicted concentration changes was good at the spine head but less satisfactory at the spine neck and dendrite. However, note in Fig. 6b that the K^+ concentration change in the spine neck had at least the right sign. The discrepancy between the electro-diffusion model and the modified cable model is larger when t_p is smaller, a condition in which concentrations are changing more quickly and are farther from equilibrium. The Nernst potential

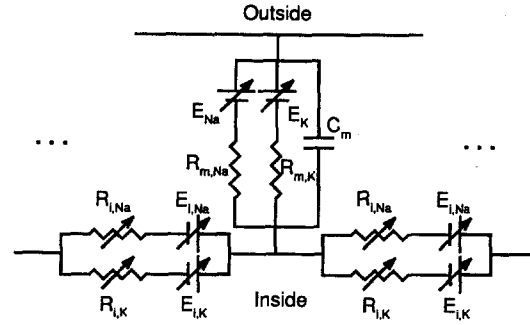


Fig. 14. Electrical circuit for a single compartment of the modified cable model. The batteries in the membrane and between compartments are calculated from the Nernst potentials and change value during a response as concentrations change. The resistivities in the cytoplasm are also updated at each time step

represents the driving force due to concentration gradient only in an equilibrium state.

9 Discussion

In most circumstances, the cable model of electrical conduction in neurons gives accurate predictions for membrane potentials during transient electrical events. A tiny amount of charge is enough to cause a substantial change in the membrane potential because the membrane capacitance is small, and as a consequence the ionic concentrations usually are nearly constant. However, the *individual* concentrations of certain ions could change significantly as long as changes in the total charge are nearly balanced out. This is more likely to happen in very small structures such as dendritic spines and for an ion such as Ca^{2+} , which is normally maintained at a very low concentration inside a cell. Thus, the predictions from the cable model should not be used without a careful analysis.

In this paper, we have developed a one-dimensional electro-diffusion model of electrical conduction which reduces to the cable model when ionic concentrations are approximately constant. This model was used to study changes in ion concentrations and membrane potentials in dendritic spines in responses to synaptic inputs. We found that ionic concentrations changed considerably in many circumstances. Thus, significant errors can be made in estimating membrane potentials and concentration changes using the cable model if the effects of diffusion and the changes in the driving forces for membrane currents are not taken into account.

On dendritic spines, these effects reduce the amplitude of excitatory postsynaptic potentials generated by Na^+ currents, and they make inhibitory inputs gen-

erated by K^+ and Cl^- currents nearly ineffective. The temporal summation of synaptic potentials is much weaker according to electro-diffusion model so multiple synaptic inputs in close succession will only make the response at the cell soma longer but not much larger. The cable model also exaggerates the veto effect of inhibition on an excitatory input when both occur on the same spine.

All these results can be understood as a consequence of changing ionic concentrations and shifting equilibrium potentials. The postsynaptic responses are mainly determined by the ionic species with the largest transient membrane permeability. Regardless of the equilibrium potential for this species (excitatory or inhibitory), the opening of channels with sufficient duration will shift the equilibrium potential of the synapse toward zero because of the large concentration changes. Therefore, if the equilibrium potential of the ionic species is greater than zero (Na^+ and Ca^{2+}) the cable model will overestimate the response. For ions whose equilibrium potential is less than zero (K^+ and Cl^-), the cable model makes predictions that can be qualitatively incorrect. For example, under certain conditions an inhibitory synaptic input that causes a K^+ conductance increase may in fact produce a postsynaptic depolarization.

Several authors have suggested that active currents in spines could enhance the transmission of signals down dendrites to the cell body (Shepherd et al. 1985; Perkel and Perkel 1985; Segev and Rall 1988). Their conclusion is still valid except that the amplitude of an action potential on a spine would be reduced (see Fig. 7) and active spines would have to be closer together to maintain transmission.

For synapses on large dendrites rather than on spines, we do not expect any significant difference between the electro-diffusion model and the cable model because the ionic concentration changes are negligible. Synaptic inputs on thick dendrites should not suffer the saturation caused by shifts of the Nernst potential, the absence of temporal summation, and lack of an inhibitory veto effect that we have demonstrated for synapses on spines. This raises the interesting possibility that otherwise identical synapses could have different functions depending on their location. It has been reported that during learning and development, the spine neck shortens and merges into the dendrite (Rausch and Scheich 1982; Coss and Globus 1978; Brandon and Coss 1982; Coss et al. 1980). The concentration changes in spines is caused not just by the small volume of the spine head but as well by the long, narrow spine neck which helps to maintain the large concentration changes that occur in the spine head. Thus, synapses on spines with long necks could switch to a different functional state if the neck were to

shorten sufficiently for the spine to merge with the dendritic shaft.

Ionic concentration changes are usually not explicitly considered in the cable model. Although ionic currents in the cable model can be integrated to yield concentration changes, this usually gives erroneous results (Figs. 6b and 10) even when the membrane potentials are predicted fairly well. Often, the cable model is solved first to find the membrane potentials and then diffusion processes are introduced to determine the ionic concentration changes (Gamble and Koch 1987; Yamada et al. 1989). Our model, however, considers the membrane potential and the ionic concentrations changes at the same time and thus provides a more natural and accurate way for solving the problem.

Ionic pumps and ionic exchange across the membrane could affect the predictions made by our simulations. The influence of these slow membrane processes can be estimated as follows. Assume that at rest the pump current for Na^+ or K^+ balances the resting Na^+ or K^+ membrane current. The pump current density in our model should be around $2.7 \mu A/cm^2$ based on the data in Tables 1 and 2, which is consistent with experimentally-determined pump current densities in the $\mu A/cm^2$ range (Weer and Rakowski 1984). A single excitatory postsynaptic potential lasting about 1.0 ms would produce Na^+ and K^+ concentration changes of 50 mM in the spine head. In contrast, Na-K pumps would take about 200 ms to change the ionic concentrations by a comparable amount. Since our results were based on the first few ms of the response, the inclusion of pumps will not affect our conclusions significantly.

We have also assumed that extracellular ionic concentrations were constant to simplify our calculations. Assume that the extracellular space around a spine head that is effectively available for exchange in 0.5 ms is about same as the volume of spine. Then a change of concentration in the spine head would cause an equal change with opposite sign outside the spine head. For $t_p = 0.25$ ms, the extracellular $[Na^+]$ would change from 140 mM to about 110 mM and $[K^+]$ from 4 mM to about 34 mM in about 0.5 ms. [See Yamada et al. (1989) for a similar estimate.] Although the extracellular K^+ concentration would increase by a larger factor, the maximum value of an excitatory synaptic response is mainly determined by the Nernst potential of Na^+ because the Na^+ permeability is much larger during an excitatory synaptic input. Also, glial cells are very effective in maintaining K^+ homeostasis on a longer time scale so that the actual change during maintained activity is probably less.

Thus the main effect of a limited extracellular space is on the Nernst potential of Na^+ . Based on the above

estimates, this would reduce the peak response of the postsynaptic potential by about 6 mV at the spine head. For large t_p and multiple synaptic inputs, the Na^+ concentration change is greater but is achieved over a longer period of time. The corresponding effective extracellular space around the spine head would then be larger because more time allows ions to diffuse farther. Thus, the modification would not be much greater. For an excitatory input driven by a Na^+ current, the effects of restricted extracellular space always reduce the amplitude of response and thus will tend to make the differences with the cable model even greater.

For interactions between excitation and inhibition on a spine or a thin dendrite, the change in concentration of extracellular K^+ can no longer be neglected because of the large K^+ permeability caused by the inhibition. However, extracellular K^+ accumulation further reduces the veto effect of inhibition. In general, extracellular concentration changes always produce effects in the same direction as the intracellular concentration changes, as discussed at the beginning of this section.

The effects of restricted extracellular space, ionic pumps, and ionic buffers can be easily included in our model when the ionic concentrations are updated, but only if the relevant parameters are available from experiments. These factors are essential for models that treat the diffusion of intracellular Ca^{2+} ions (Fogelson and Zucker 1985; Simon and Llinas 1985; Stockbridge and Moore 1984; Yamada et al. 1989).

We used an explicit method to solve the electro-diffusion equations. Very small time step had to be used to make the calculation stable and therefore the simulation was much slower than cable model. This problem can be partly alleviated by using an implicit method of integration (Mascagni 1989). The modified cable model introduced in the last section was much faster (see Appendix). However, the modified cable model may not be able to accurately predict the concentration changes in the spine neck and the dendrite, and its predictions of interactions between excitation and inhibition may also be seriously in error in some circumstances. The electro-diffusion model should be used whenever accurate estimates are needed.

Appendix

Derivation of (7)

In cylindrical coordinates (ρ, ϕ, z) , (6) becomes:

$$\frac{1}{\rho} \frac{\partial(\rho J_{k,\rho})}{\partial \rho} + \frac{\partial J_{k,z}}{\partial z} + \frac{1}{\rho} \frac{\partial J_{k,\phi}}{\partial \phi} + \frac{\partial n_k}{\partial t} = 0. \quad (\text{A1})$$

For a cylindrically-symmetric neuronal process, $J_{k,\phi} = 0$, and all the variables are independent of ϕ . Integrate both sides of (A1)

over the cross sectional area of the process, assuming that $J_{k,z}$ and n_k are independent of ρ :

$$\frac{4}{d} J_{k,\rho}|_{\rho=d/2} + \frac{\partial J_{k,z}}{\partial z} + \frac{\partial n_k}{\partial t} = 0, \quad (\text{A2})$$

where $J_{k,\rho}|_{\rho=d/2}$ is the membrane flux of ionic species k , $J_{m,k}$. The ρ and z components of (5) can be written as:

$$J_{k,\rho} = -D_k \left(\frac{\partial n_k}{\partial \rho} + \frac{n_k}{\alpha_k} \frac{\partial V}{\partial \rho} \right), \quad (\text{A3})$$

$$J_{k,z} = -D_k \left(\frac{\partial n_k}{\partial z} + \frac{n_k}{\alpha_k} \frac{\partial V}{\partial z} \right). \quad (\text{A4})$$

Equation (7) is obtained by inserting (A4) into (A2). Equation (A3) can be integrated under the constant field approximation (Goldman 1943) to obtain (8).

Membrane Potential at a Diameter Jump or Branch Point

Consider Fig. 15 in which the diameter of a process changes from d_1 to d_2 within a short distance ϵ . As $\epsilon \rightarrow 0$, there is a discontinuity, or diameter jump at $z=0$. The potential at the jump is:

$$V(0, t) = \lim_{\epsilon \rightarrow 0} \frac{1}{\epsilon} \int_0^\epsilon V(z, t) dz. \quad (\text{A6})$$

From (10), this becomes:

$$V(0, t) = V_{\text{rest}} + (F/4C_m) \times \left[\lim_{\epsilon \rightarrow 0} (1/\epsilon) \int_0^\epsilon d(z) dz \right] \sum_k [n_k(z, t) - n_{k,\text{rest}}] z_k, \quad (\text{A7})$$

where the spatial variable z should not be confused with valence z_k . For small z we can use a linear approximation for $d(z)$:

$$d(z) = d_1 + (d_2 - d_1)z/\epsilon.$$

This expression can be substituted into (A7) to obtain:

$$V(0, t) = V_{\text{rest}} + (F/4C_m) [(d_1 + d_2)/2] \sum_k [n_k(z, t) - n_{k,\text{rest}}] z_k, \quad (\text{A8})$$

which is the average of the potentials on both sides of diameter jump. This result can be generalized to the branching case shown in Fig. 2: The branching point is then the average of the potentials in all three branches.

Numerical Methods

We used an explicit method to integrate the electro-diffusion equations. For a small time step Δt and spatial sample points separated by Δz , the one-dimensional electro-diffusion (9) re-

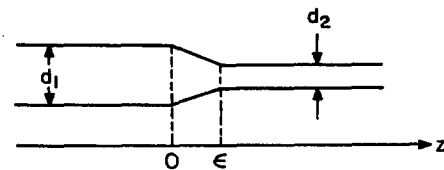


Fig. 15. Jump in dendritic diameter from d_1 to d_2 over distance ϵ

duces to the following difference equation:

$$n_{j,t} = \left\{ n_j + \frac{D\Delta t}{(\Delta z)^2} (n_{j+1} + n_{j-1} - 2n_j) + \frac{D\Delta t}{\alpha} \frac{(n_{j+1} + n_j)(V_{j+1} - V_j) - (n_j + n_{j-1})(V_j - V_{j-1})}{2(\Delta z)^2} - \frac{4PV_j\Delta t}{\alpha d} \left[\frac{n_j^{\text{out}} - n_j \exp(V/\alpha)}{1 - \exp(V/\alpha)} \right] \right\} \Big|_{t-\Delta t} \quad (\text{A9})$$

The subscript k for different ionic species has been omitted for clarity. The subscript j refers to spatial sample points along the neuronal process. Assume at the boundaries of the process that the flux of each ion is zero. Using (10), the matching condition, (11), for the branch point in Fig. 2 can be written as:

$$(d_1/2\Delta z_1) \left[(n_{k,0} - n_{k,1}) + Az_k n_{k,0} \sum_k z_k (n_{k,0} - n_{k,1}) \right] + (d_2/2\Delta z_2) \left[(n_{k,0} - n_{k,2}) + Az_k n_{k,0} \sum_k z_k (n_{k,0} - n_{k,2}) \right] + (d_3/2\Delta z_3) \left[(n_{k,0} - n_{k,3}) + Az_k n_{k,0} \sum_k z_k (n_{k,0} - n_{k,3}) \right] = 0, \quad (\text{A10})$$

where Δz_j ($j=1, 2, 3$) is the length of the spatial compartments, z_k is the valence of ionic species k , $n_{k,j}$ is the concentration of ionic species k at spatial location j (see Fig. 2), $A = F^2\bar{d}/4RTC_m$ and $\bar{d} = (d_1 + d_2 + d_3)/3$.

Equation (A10) is a set of coupled nonlinear algebraic equations that can be solved using Newton's method. The solution at the previous time step can be used as the initial guess. For the special case in which all the ionic species considered have the same charge, z_k , the closed form solution can be obtained easily by first adding all the equations together and defining

$$n_i = \sum_k n_k.$$

A Ridge 32 (equivalent to a VAX 780 FPA) was used to solve these finite difference equations. The calculations were performed for space and time steps of successively smaller size and the values reported were ones for which further decrease to the step sizes made less than 2% difference to the solution. In our simulation of dendritic spines, sample points in the dendrite were 10 μm apart and the integration time step was 10^{-7} s; in the spine head and neck the spacing was 0.173 μm and 0.167 μm respectively and the time steps were 2×10^{-9} s. The model had a total of 41 sample points: 31 in the dendrite, 6 in the spine neck, and 4 in the spine head. About 30 min was required to integrate 1 ms of real time. In the standard and modified cable models, only 33 lumped compartments were used (1 for head, 1 for neck, and 31 for dendrite) due to the large space constant. The time step for the spine head and neck was 10^{-7} s and that for the dendrite was 10^{-6} s. The standard cable model took 26 s to integrate 1 ms of real time and the modified cable model required 1 min.

Relationship Between the Cable Model and the Electro-Diffusion Model

We show here that (7) and (10) are equivalent to (1) in the limit of small concentration gradients. When the cytoplasmic ionic concentration gradients are small, $\partial n_k/\partial z$ is approximately zero. The first term on the right side of (7) can then be neglected, so that:

$$\frac{\partial n_k}{\partial t} = \frac{D_k}{\alpha_k} n_k \frac{\partial^2 V}{\partial z^2} - \frac{4}{d} J_{m,k}. \quad (\text{A11})$$

Multiply both sides of (A11) by $z_k F d / 4 C_m$, sum over all i , and apply (10) to obtain:

$$\frac{d}{4} \sum_k \frac{F^2}{RT} D_k n_k z_k^2 \frac{\partial^2 V}{\partial z^2} = C_m \frac{\partial V}{\partial t} + \sum_k z_k F J_{m,k}. \quad (\text{A12})$$

Notice that $\sum_k z_k F J_{m,k}$ is exactly the total membrane current per unit area I_m , so that Equation (A12) and (1) are identical if we let

$$1/R_i = (F^2/RT) \sum_k D_k n_k z_k^2. \quad (\text{A13})$$

Equations (12) and (13) are obtained by assuming that the total cytoplasmic resistivity R_i in the electrical conductance model is due to the contribution from each type of ionic species k . Equation (A13) can be also obtained, more easily, by considering the longitudinal current expressions in the two models.

Acknowledgements. We are grateful to Drs. Julian Jack, Wilfrid Rall, John Rinzel, and Christof Koch for helpful comments on earlier versions of this paper. We also thank several referees for suggesting improvements. This research was supported by grants from the National Science Foundation and the Mathers Foundation.

References

- Brandon JG, Coss RG (1982) Rapid dendritic spine stem shortening during one-trial learning: the honeybee's first orientation flight. *Brain Res* 252:51-61
- Cooley JW, Dodge FA (1966) Digital computer solutions for excitation and propagation of the nerve impulse. *Biophys J* 6:583-599
- Coss RG, Globus A (1978) Spine stems on tectal interneurons in jewelfish are shortened by social stimulation. *Science* 200:787-789
- Coss RG, Perkel DH (1985) The function of dendritic spines. *Behav Neur Biol* 44:151-185
- Coss RG, Brandon JG, Globus A (1980) Changes of morphology of dendritic spines on honeybee calycal interneurons associated with cumulative nursing and foraging experiences. *Brain Res* 192:49-59
- Fogelson AL, Zucker RS (1985) Presynaptic calcium diffusion from various arrays of single channels. *Biophys J* 48:1003-1017
- Frankenhaeuser B, Huxley AF (1964) The action potential in the myelinated nerve fiber of *Xenopus laevis* computed on the basis of voltage clamp data. *J Gen Physiol* 171:302-315
- Gamble E, Koch C (1987) The dynamics of free calcium in dendritic spines in response to repetitive synaptic input. *Science* 236:1311-1315
- Goldman DE (1943) Potential, impedance and rectification in membranes. *J Gen Physiol* 27:37-60
- Hille B (1984) Ionic channels of excitable membranes. Sinauer, Sunderland, Mass
- Hodgkin AL, Huxley AF (1952) Currents carried by sodium and potassium ions through the membrane of the giant axon of *Loligo*. *J Physiol* 116:449-472
- Jack JJB, Noble D, Tsien RW (1975) Electrical current flow in excitable cells. Oxford University Press, Oxford
- Koch C, Poggio T (1983) A theoretical analysis of electrical properties of spines. *Proc R Soc London B* 218:455-477
- Koch C, Poggio T, Torre V (1983) Nonlinear interaction in a dendritic tree: location, timing, and role in information processing. *Proc Natl Acad Sci USA* 80:2799-2802

- Malenka RC, Kauer JA, Zucker RS, Nicoll RA (1988) Postsynaptic calcium is sufficient for potentiation of hippocampal synaptic transmission. *Science* 242:81–84
- Mascagni MA (1989) Numerical methods for neuronal modeling. In: Koch C, Segev I (eds) *Methods in neuronal modeling*. MIT Press, Cambridge
- Perkel DH, Perkel DJ (1985) Dendritic spines: role of active membrane modulating synaptic efficacy. *Brain Res* 325:331–335
- Qian N, Sejnowski TJ (1988) Electro-diffusion model of electrical conduction in neuronal processes. In: Woody CW, Alkon DL, McGaugh JL (eds) *Cellular mechanisms of conditioning and behavioral plasticity*. Plenum Press, New York
- Qian N, Sejnowski TJ (1989) Inhibition on spines and thin dendrites may be ineffective because of ionic concentration changes. *Soc Neurosci (abstr)* 15
- Rall W (1967) Distinguishing theoretical synaptic potentials computed for different soma-dendritic distribution of synaptic input. *J Neurophysiol* 30:1136–1168
- Rall W (1977) Core conductor theory and cable properties of neurons. In: Kandel ER (ed) *Handbook of physiology: the nervous system*. American Physiological Society, Bethesda, Md, pp 39–97
- Rall W (1978) Dendritic spines and synaptic potency. In: Poeter R (ed) *Studies in neurophysiology*. Cambridge University Press, Cambridge
- Rall W, Segev I (1987) Functional possibilities for synapses on dendrites and dendritic spines. In: Edelman GM, Gall WF, Cowan WM (eds) *New insights into synaptic function*. Wiley, New York
- Rausch G, Scheich H (1982) Dendritic spine loss and enlargement during maturation of the speech control system in mynah bird (*Gracula religiosa*). *Neurosci Lett* 29:129–133
- Segev I, Rall W (1988) Computational study of an excitable dendritic spine. *J Neurophysiol* 60:499–523
- Shepherd GM, Brayton RK, Miller JP, Segev I, Rinzel J, Rall W (1985) Signal enhancement in distal cortical dendrites by means of interactions between active dendritic spines. *Proc Natl Acad Sci USA* 82:2192–2195
- Simon SM, Llinas RR (1985) Compartmentalization of the submembrane calcium activity during calcium influx and its significance in transmitter release. *Biophys J* 48:485–498
- Stockbridge N, Moore JW (1984) Dynamics of intracellular calcium and its possible relationship to phasic transmitter release and facilitation at the frog neuromuscular junction. *J Neurosci* 4:803–811
- Wathley J, Lytton W, Jester J, Sejnowski T (1989) Simulations of synaptic potentials using realistic models of hippocampal pyramidal neurons. *Soc Neurosci (abstr)* 15
- Weer PD, Rakowski RF (1984) Current generated by backward-running electrogenic Na⁺ pump in squid giant axons. *Nature* 309:450–452
- Yamada WM, Koch C, Adams PR (1989) Multiple channels and calcium dynamics. In: Koch C, Segev I (eds) *Methods in neuronal modeling*. MIT Press, Cambridge

Received: October 16, 1988

Accepted in revised form: June 27, 1989

Dr. Terrence Sejnowski
Computational Neurobiology Laboratory
The Salk Institute
P.O. Box 85800
San Diego, CA 92138-9216
USA